Chapter 6

Comparison of Particle Filter Variants towards RUL Estimation

6.1 Introduction

The present study contributes to the development of a robust prognostic approach to assess life of a motor. A comparison of the different data driven approaches has been addressed long back by the researchers of PHM community (Adhikari et al. 2018; An et al. 2013b; Kai Goebel, Bhaskar Saha 2008; Walker et al. 2015). Results and discussion from the earlier chapter 5 helped to finalize the adaptive filtering approach as a superior technique in comparison to the exponential degradation method (Banerjee et al. 2021). However, the present chapter shall testify the superiority of the *i*-UPF amongst the other PF variants keeping in mind the improved RUL accuracy estimates.

The research works (Jouin et al. 2016) employ two ways to distinguish engaging with nonlinearity and noise processing while maneuvering PF. Crack localization studies were conducted by comparing the degraded signals from the wing box of an A320 airbus using wavelet transform (Celaya et al. 2012). Physics based prognostics (hybrid modeling) approach for similar types of crack growth problems was dealt with by An et al. (2013a). A comparison of the developed code and the RUL results were performed with a Li-ion battery dataset. In dealing with the problem of track degradation in railroads, PF's comparison with a typical regression technique provided a highly accurate outcome (Mishra et al. 2017). Baltatanu and Marin Florea (2013) compared eight electric motors addressing their present day deliverables and the demand for electric vehicle propulsion technology. Their study addresses the techno-economic excellence made based on the performance of engine and electric batteries. The nondestructive control methodology aided in dynamically configuring the algorithm to monitor the critical structures by localizing flaws present in a much rapid pace. The use of PF variants along with the resampling extends their use to visual tracking by target tracking the observer in a video sequence and reducing image size. The application dealt with the use of lesser number of particles and processing time thereby overcoming ten different challenges and aiding to the smart monitoring applications (Moghaddasi and Faraji 2020). The rise in electrical utilities in vehicles incorporated the use of PF alongside the autoencoders (Jiao et al. 2020).

Extensive use of resampling techniques alongside particle distribution optimization to alleviate particle degeneracy was focused and RUL results were dealt with the use of conditional variational autoencoder (Jiao et al. 2020). The results were found to be superior while computation time was much higher when compared to any of our PF variants. Similar accuracy in RUL results for the present case study have been obtained using the improved variant of PF that has been addressed in the present chapter. Prior to the selection of the best variant out of the PF, UPF and *i*-UPF technique, the best choice of resampling out of the four (systematic, residual, multinomial, and stratified) resampling approaches needs to be finalized. The UPF and *i*-UPF considers all parameters in the state estimation process whilst with the exception of the Gaussianity constraint. The practice of resampling strategy besides empirical degradation modeling has been more focused on prognostic health management programs.

The main theme of the work is predicting an accurate motor RUL. The subsequent section elaborately discusses the results of resampling. Next to the resampling stands the appropriate choice of the *c*-value. The *c*-value helps in finalizing the two-step framework in selecting the number of particles for obtaining a posterior function in case of *i*-UPF. The second part of the chapter concludes with the verification and validation of the results with our developed algorithm using the benchmark NASA, PCoE lithium-ion battery data.

6.2 Results and Discussion

6.2.1 Comparative Results of Resampling Study

In the case of PF, the prediction is followed by a correction step. The initial sampling step produces a measure of the target for each particle. Considering the weights of each particle, the final state is predicted. The likely difference between the measured and the estimated state leads to weight updating. A lower weighted particle is found when the estimation error in the results is higher. Furthermore, a decrease in the effective samples size leads to particle degeneracy. The adherence to the lower weight particles shall generate an inferior estimate of the posterior densities. Implementation of the resampling phenomenon helps in completely evading the inferiority in the results. Resampling adopts heavy-weight particles by eliminating the low-weight particles to produce a precise estimate of the state. Besides, the resampling takes care of nonlinearity, while noise in the data has been treated by ignoring the less weighted particles.

However, in motor state prediction and assessment using PF, less periodic evidence from previous works (Jouin et al. 2016) has been discovered, creating additional space for motor prognosis. To overcome the inherent problem of sample degeneracy, the present chapter emphasizes the improvements in the RUL estimation results by incorporating four resampling (Guo et al. 2015a) techniques within the three PF variants (PF, UPF and *i*-UPF) and incorporating upon three different experimental datasets. Comparison of the resampling results using two metrics namely the ESS and RUL_error (Guo et al. 2015b). With the favorable resampling technique, the computational accuracy for the three different PF variants with real-time motor datasets has been found. Resampling forbids a loss of diversity (Bacak and Köksal Hocaoğlu 2020) for a population of particles and reduces the computational cost. Therefore, a trade-off can be seen for a loss in diversity and the computational cost associated with a finite accuracy in RUL results. The superiority of the prognostic method is finalized employing RUL_error (i.e., relative percentage error) values and plays a vital role in selecting the best resampling technique.

Assuming T_t^i is the end-of-life of the motor predicted by an *i*-th particle, so the RUL_t can be expressed as $RUL_t^i = (T_t^i - t) \qquad i = 1,....N$ (6.1)

The relative prediction error can be expressed as:

$$\text{RUL\_error} = \frac{\left|(trueRUL) - mean(RUL)\right|}{trueRUL} \tag{6.2}$$

Performance is quantified by observing the error of the mean RUL estimates. Comparison of the results also demonstrates the effectiveness of the PF variants in aggregating information from training data and its efficacy in motor RUL prediction under transient loading conditions.

The choice of higher ESS (*N-eff*) is a measure of efficient resampling. The measure of the correlation between the observed weights and the particles is defined as ESS. The second measure of performance is in quantifying the ESS. The lower the value of ESS, the severe is the degeneracy. Resampling is encountered when the ESS of the particles is below a set threshold (*N-th*) i.e., $N-eff < N-th$ to alleviate particle degeneracy. Tests for 500 simulations were carried out for selecting the best resampling when used with *i*-UPF, UPF and PF techniques. To attain an optimal global solution, Moghaddasi and Faraji (2020) used a genetic algorithm to compute ESS. Self-fission based deterministic unbiased resampling (Li et al. 2012b) were employed to get rid of particle impoverishment.

Table 6.1 comprises the results of resampling methods for the Strategy-I experimental dataset for 500 simulations. The 500 iterations for a sequence of operations in repetitive mode

would successively result in a robust estimate. Present work incorporates the measure of RUL_error and the ESS in finding the superiority of the resampling technique. The proposed work is aimed towards the development of an efficient prognostic methodology while computing the clutch motor's RUL. Performance has been measured in terms of computational time and a comparison of the three PF variants by making use of three experimental datasets are derived.

Table 6.1 Comparison of Quantitative Resampling Results from Strategy-I

Particle Filter				
	Resampling Methods			
Metrics	Systematic	Residual	Multinomial	Stratified
ESS	101	100	97	99
RUL_error	0.436	0.438	0.438	0.439
Computational Time	2.9886			
Unscented Particle Filter				
	Resampling Methods			
Metrics	Systematic	Residual	Multinomial	Stratified
ESS	337	331	339	333
RUL_error	0.094	0.094	0.094	0.094
Computational Time	16.2439			
Improved Unscented Particle Filter				
	Resampling Methods			
Metrics	Systematic	Residual	Multinomial	Stratified
ESS	297	294	299	297
RUL_error	0.066	0.066	0.066	0.066
Computational Time	8.2604			

For a likelihood of normally distributed phenomenon, the systematic resampling outperformed in the case of PF, while multinomial resampling is mainly favored for UPF and *i*-UPF. While implementing on a Strategy I degradation motor dataset, all three variants of PF exhibit similar changes in findings of RUL_error. A slight change in ESS values is found for each variant of PF. The ESS shares a functional relationship between the observations and the particles mutually. The equivalent size of the ESS refers to the likelihood of information for the observed

dataset. The higher the magnitude, the higher the likelihood of the particles getting used in the prediction process. This, in turn, helps in decreasing particle redundancy. Similar results can be observed in Fig. 6.1, which compares RUL_error for all four resampling methods across 500 iterations using *i*-UPF.

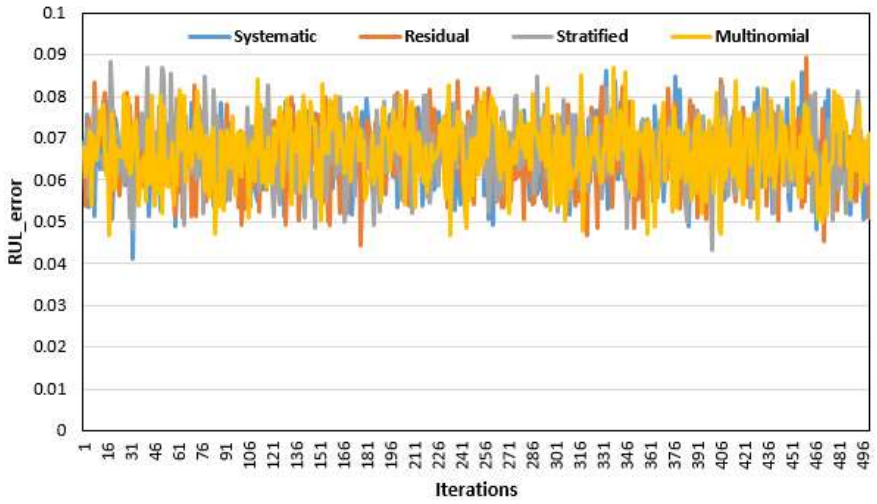

Figure 6.1 Comparison of resampling plots in case of *i*-UPF for Strategy-I dataset

Fig. 6.1 addresses the superiority of multinomial resampling in *i*-UPF and their choice in state prediction followed by RUL estimation. An excellent trade-off between the computation time and accuracy in results of *i*-UPF was found using multinomial resampling. However, the precision level has been higher in the case of PF and UPF. For multinomial resampling, the estimated RUL_error has been consistent for the PF, while the magnitude of error is significantly lower for UPF and *i*-UPF which resembles an improved estimate of RUL.

A similar technique has been adopted for the Strategy-II dataset to compare the superiority of the multinomial resampling and its role in state prediction. Test results in Table 6.2 were obtained after 500 runs and quantification of the accuracy is attained via plots of RUL_error, while computing the motor RUL.

Table 6.2 Comparison of Quantitative Resampling Results from Strategy-II

Particle Filter				
	Resampling Methods			
Metrics	Systematic	Residual	Multinomial	Stratified
ESS	26	25	27	26

RUL_error	0.202	0.202	0.199	0.200
Computational Time	1.6497			
Unscented Particle Filter				
	Resampling Methods			
Metrics	Systematic	Residual	Multinomial	Stratified
ESS	255	250	260	248
RUL_error	0.475	0.475	0.475	0.475
Computational Time	4.0291			
Improved Unscented Particle Filter				
	Resampling Methods			
Metrics	Systematic	Residual	Multinomial	Stratified
ESS	209	208	215	210
RUL_error	0.420	0.420	0.423	0.421
Computational Time	6.2396			

The use of 1000particles and a 95% confidence interval have been favored for RUL estimation. Using the Strategy-II dataset, the multinomial resampling has been found to be superior for all the three PF variants. Fig. 6.2 illustrates the comparison of the RUL_error plots for all the four resampling methods and *i*-UPF method. The *i*-UPF using a considerable amount of particles effectively made use of the multinomial resampling by generating a lower RUL_error value.

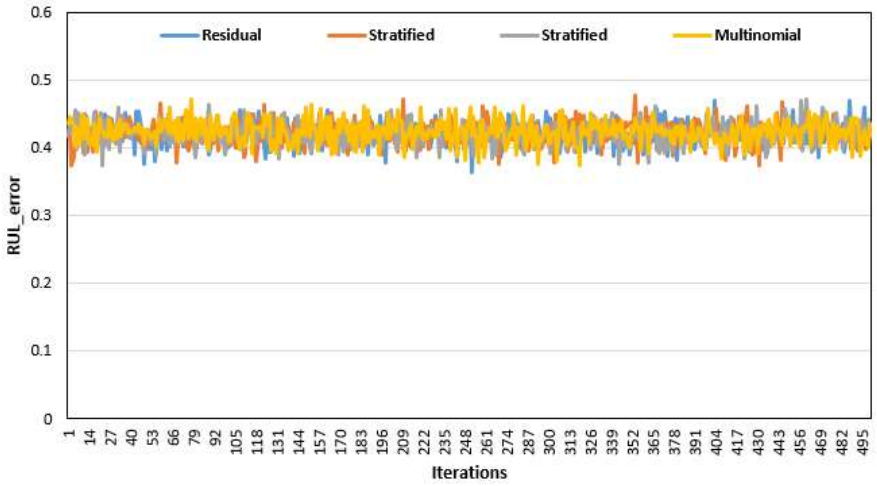

Figure 6.2 Comparison of resampling plots in case of *i*-UPF for Strategy-II dataset

Table 6.3 shows the resampling results for 500 iterations using the Strategy-III dataset. A systematic evaluation of the three PF variants reveals that the preferred choice is multinomial for PF, systematic for UPF, and multinomial resampling for *i*-UPF. Maximized efficiency in the RUL results has been obtained using multinomial resampling for all three experimental strategies.

Table 6.3 Comparison of Quantitative Resampling Results from Strategy-III

Particle Filter				
	Resampling Methods			
Metrics	Systematic	Residual	Multinomial	Stratified
ESS	192	190	193	190
RUL_error	1.435	1.436	1.435	1.437
Computational Time	3.2193			
Unscented Particle Filter				
	Resampling Methods			
Metrics	Systematic	Residual	Multinomial	Stratified
ESS	308	304	302	302
RUL_error	1.336	1.338	1.336	1.335
Computational Time	17.2134			
Improved Unscented Particle Filter				
	Resampling Methods			
Metrics	Systematic	Residual	Multinomial	Stratified
ESS	277	269	277	275
RUL_error	1.357	1.357	1.355	1.355
Computational Time	9.2368			

Fig. 6.3 illustrates RUL_error for the four resampling methods used in the case of *i*-UPF to provide an efficient RUL estimate. Table values computed for the Strategy-I and Strategy-II datasets reflect a significantly smaller ESS value in the state prediction scheme while using PF. However, a higher magnitude of ESS is reflected in the results that assist in generating an approximated posterior density function while using UPF and *i*-UPF schemes.

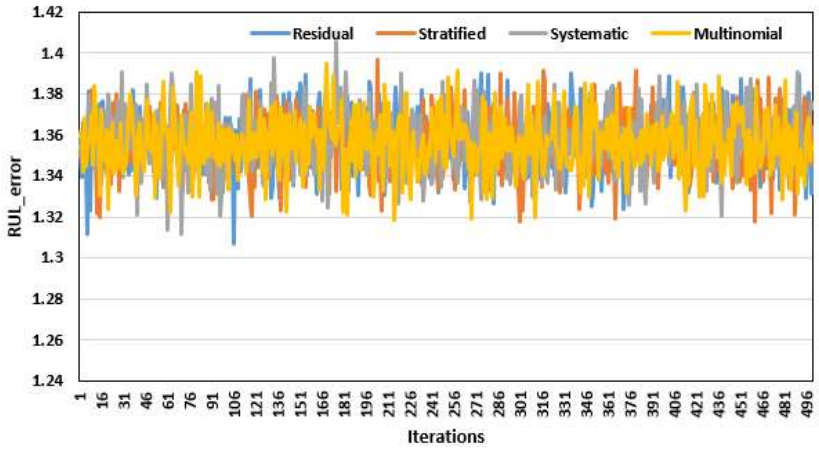

Figure 6.3 Comparison of resampling plots in case of *i*-UPF for Strategy-III dataset

Resampling replaces the set of particles with another set of corresponding particle weights. The property of unbiasedness in sampling (Li et al. 2015b) had been a significant dominance of the method. The order of computational complexity is much higher in the case of multinomial and lower for systematic resampling. The present study provides an efficient choice of resampling based on the measure of RUL_error and the ESS for each of the four resampling techniques.

6.2.2 Optimal Choice of *c*-value

Results from the previous three strategies reflect the dominance of *i*-UPF in RUL prediction. The ESS metric for all the three variants of PF has been found to be maximum in UPF. However, the choice of accurate RUL depends on the minimum RUL_error value. The *i*-UPF depends on the optimal choice of *c*-value (details of *i*-UPF has been discussed in sub-section 4.4.2 of Chapter 4). The choice in the magnitude of the *c*-value has been cumbersome, which differentiates all three variants of PF. For a traditional PF and UPF, the *c*-value has been chosen 0 and 1, respectively. An appropriate choice for the *i*-UPF methodology has been adopted by evaluating the standard deviation of the RUL for a range of *c*-values from 0 to 1.

Fig. 6.4 - 6.6 clearly indicates that the lowest value of the mean of standard deviation of RUL at respective *c*-values of 0.55, 0.45 and 0.45 respectively. The *i*-UPF makes use of a significant amount of the data in generating the particles via UT. With the introduction of a new parameter '*c*' the particle generation is segregated into two parts. The particles for one part are generated from the transition prior while the other part uses the UKF. The results were computed for 500runs and the mean values were considered for generating the respective plots.

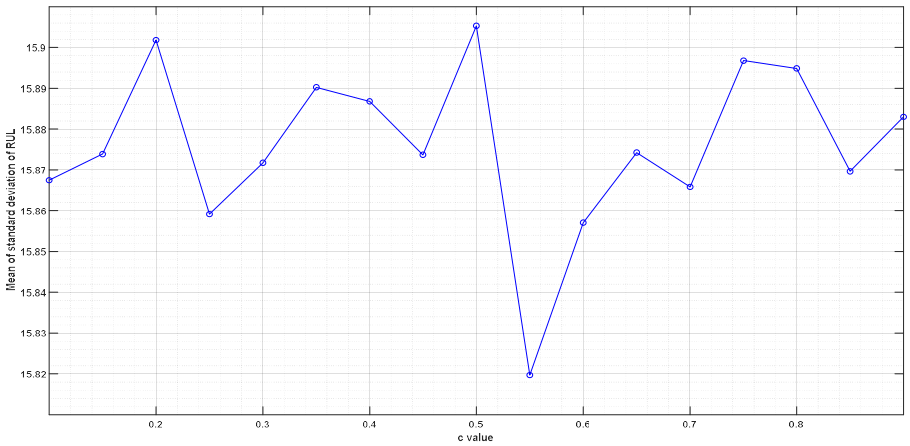

Figure 6.4 Optimal choice of *c*-value for Strategy-I

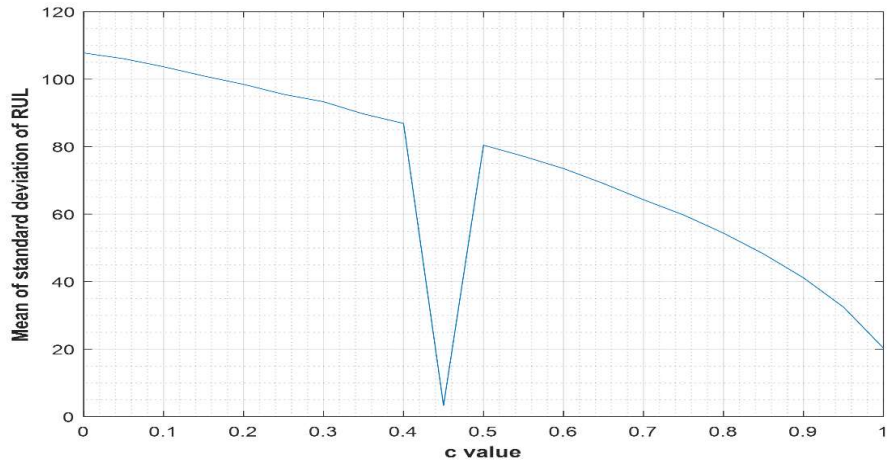

Figure 6.5 Optimal choice of *c*-value for Strategy-II

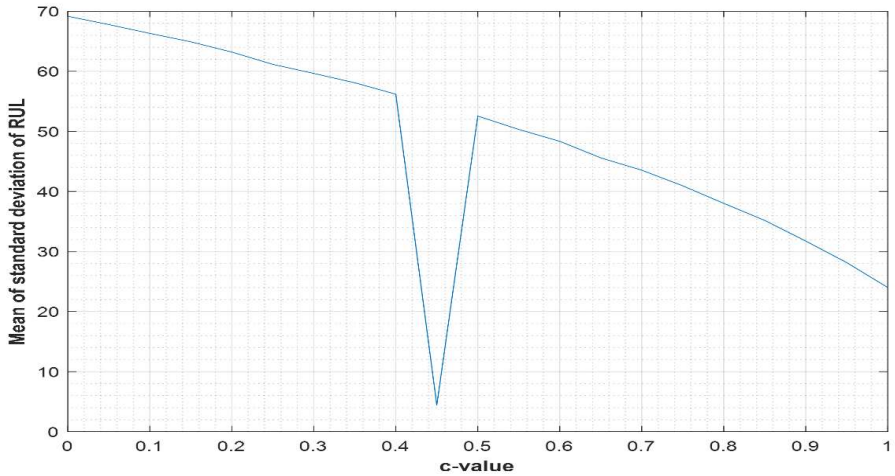

Figure 6.6 Optimal choice of *c*-value for Strategy-III

The computational time is seen to decrease with the introduction of the *i*-UPF when compared to traditional UPF. The optimal choice of '*c*-value' has been carried out for 500 runs and a value of 0.55, 0.45 and 0.45 has been finally accepted for further analysis. The selection of parameter '*c*-value' was indeed based on the standard deviation of the RUL. The subsequent section elaborates the results of motor RUL and their accuracy for the three experimental datasets. The 319cycles Strategy-I dataset, the 249cycles Strategy-II dataset and the Strategy-III dataset comprising of 520cycles. Details of the three datasets has been discussed earlier in section 5.2.1 of Chapter5.

6.2.3 Comparative RUL prediction results of Strategy–I dataset

The fulfillment of the primary aims, i.e., the accuracy, robustness and ease of computational complexity, has been achieved. A larger number of particles has been aimed towards accuracy, while a lesser number of particles has helped to achieve the computational benefits. Experiments were conducted using different particle sets and a set of 1000 particles provided the improved RUL results. Table. 6.4 below summarizes the choice of best resampling method for each of the PF variants along with the optimal '*c*-value' that has been used for motor RUL prognosis.

Table 6.4 Choice of best Resampling for Strategy-I dataset

	***c*-value**	**Resampling Methods**	**True RUL**	**Mean RUL**
PF	0	Systematic	127	117
UPF	1	Multinomial	127	134
i-UPF	0.55	Multinomial	127	131

The mean RUL resembles the mean computed over 500 iterations. The mathematical description for the proposed adaptive filtering methodology can be found in section 4.3 of chapter 4, which explains the underlying process's schematic. The comparative prediction plots for the three methods, such as the traditional PF, UPF, and *i*-UPF, can be seen in Fig. 6.7.

The RUL pdf (see Fig. 6.7) resembles a Gaussian with a precise peakedness that depicts the precision of the calculated RUL within the confidence bounds shown by dashed lines (the upper and lower bound). The vertical line represents the end of the training dataset, while the horizontal line is the failure threshold, i.e., 3.51. Prediction continues till the predicted state reaches the threshold, and RUL is evaluated by subtracting the current time from the failure time. Robustness in the RUL prediction results was evident with respective resampling methods, and the *i*-UPF had been the most accurate among the three PF methods. Three different color

combinations are used to compare the motor RUL accuracy for three PF variants. The histogram of the RUL pdf is found to be the same as obtained in section 5.3.4 of Chapter 5.

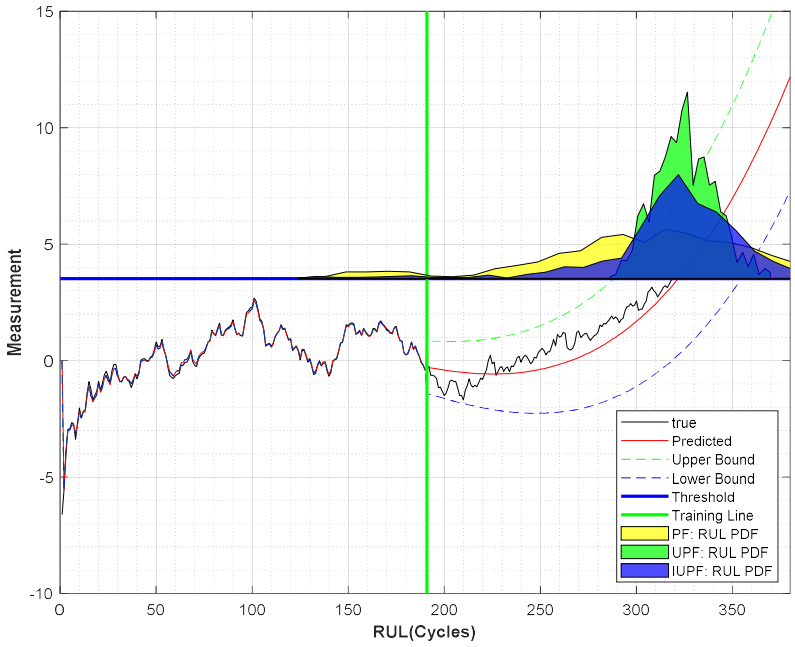

Figure 6.7 Comparison of PF, UPF and *i*-UPF using Strategy-I dataset for motor RUL prediction

It has been essential to note that the criticality in predicting failure was higher near the end of life than the beginning. This is due to the use of parameter values for only 60% training dataset. Prediction is said to continue without further updating of the parameters. The maximum value of the dataset has been the pre-set failure point or the threshold in the dataset. The *i*-UPF provided a robust estimate of RUL (131) amongst all three PF variants.

6.2.4 Comparative RUL prediction results of Strategy–II dataset

Exhaustive computation for 500 iterations were conducted for estimating the motor RUL making use of a 249 cycles Strategy-II dataset. However, the fulfillment of RUL accuracy within less computational time has been achieved. The mean RUL values in Table 6.5 for the Strategy-II dataset show that the findings are reasonably similar, which might be attributed to nonlinear noise. This may be due to the smaller size of dataset with the presence of very high fluctuations.

Table 6.5 Choice of best Resampling for Strategy-II dataset

	***c*-value**	**Resampling Methods**	**True RUL**	**Mean RUL**
PF	0	Multinomial	99	79
UPF	1	Multinomial	99	83

i-UPF	0.45	Multinomial	99	84

The comparative state prediction plots in Fig. 6.8 for the three PF variants can be seen plotted within 95% confidence intervals. RUL results depict that for a noisy dataset, the UPF besides *i*-UPF very well handles the data.

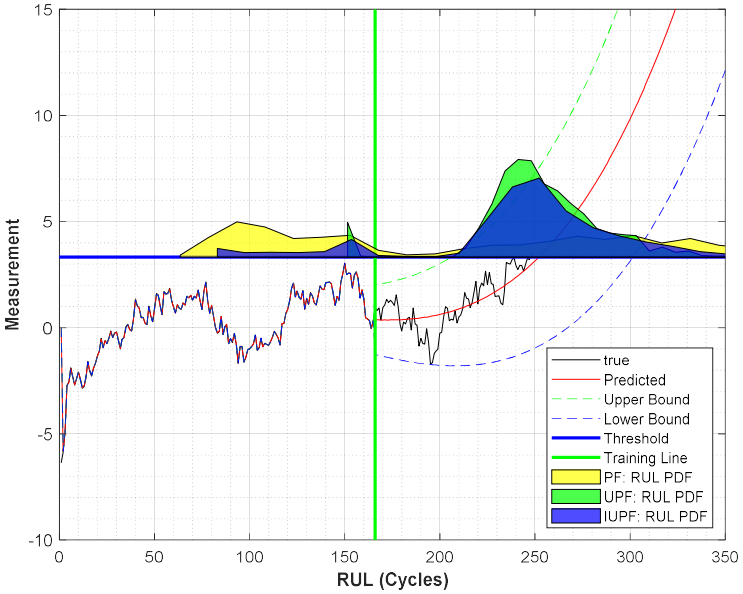

Figure 6.8 Comparison of PF, UPF and *i*-UPF using Strategy-II dataset for motor RUL prediction

6.2.5 Comparative RUL prediction results of Strategy–III dataset

The Strategy-III degradation motor dataset comprises 520cycle data. Experiments were conducted with a 60% training set and a set of 1000 particles. Table 6.6 elaborates the choice of multinomial resampling as the best, while the residual resampling was performing the worst in the motor's RUL prediction. The comparative prediction plots (see Fig. 6.9) for the traditional PF, UPF, and *i*-UPF again depict the accuracy of *i*-UPF in the state prediction scheme.

Table 6.6 Choice of best Resampling for Strategy-III dataset

	***c*-value**	**Resampling Methods**	**True RUL**	**Mean RUL**
PF	0	Multinomial	208	214
UPF	1	Multinomial	208	205
i-UPF	0.45	Multinomial	208	207

During the implementation of *i*-UPF, an inaccuracy of 1cycle was noticed in the RUL findings which were calculated within 95 percent confidence bounds. Similarly, a 3cycle error was discovered for UPF, whereas the RUL prediction using PF resulted in an overestimated outcome.

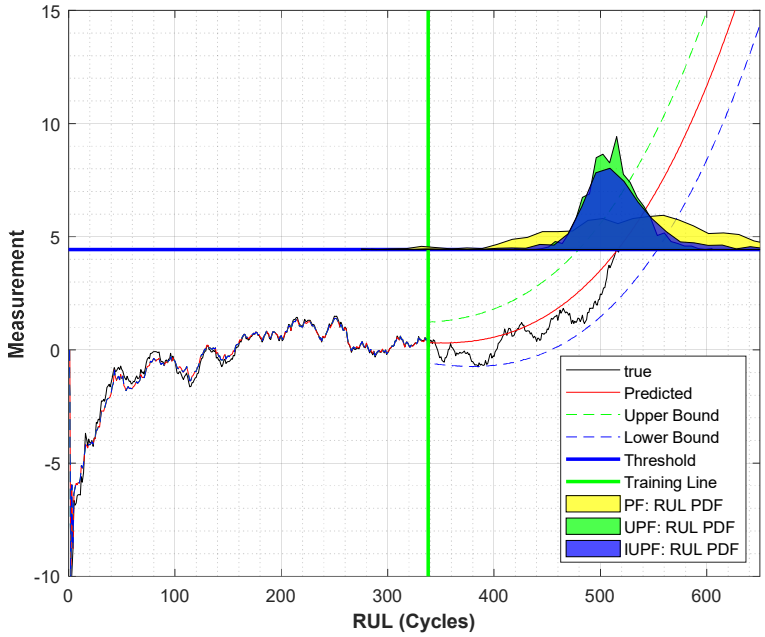

Figure 6.9 Comparison of PF, UPF and *i*-UPF using Strategy-III dataset for motor RUL prediction

Traditional PF is surpassed as UPF generates particles in a PF scheme utilizing UKF, thereby inducing better performance. However, generating proposal distribution using UKF for each particle increases the computational time. The role of *i*-UPF is to generate the proposal distribution from true mean and covariance of state for the newly transformed set of particles instead of each individual particles. In the process, the resampling utilizes the known proposal density function instead of the transition prior in case of PF to get rid of particle degeneracy. The proposed scheme generates a highly improved RUL estimate within a reduced computation time making it more practicable in non-linear applications.

In order to justify the superiority of the proposed RUL prediction scheme, verification and validation of the same has been conducted with Lithium-ion battery data from the NASA Prognostic Centre of Excellence (PCoE). The PCoE data has been considered as a benchmark data while validating any prognostic methodology and many published works from eminent researchers from PHM fraternity is in support of it. Idea of an extensive literature in context to Li-ion battery works using PCoE data can be found in the works of (Guo et al. 2015c; Olivares et al. 2013).

6.3 Verification and Validation

This present research establishes performance benchmarking for the designed model with regards to the PCoE battery data (Saha and Goebel 2007). Prognostic Data repository intends in developing prognostics algorithms using battery datasets from PCoE at NASA Ames. The presently used dataset has been downloaded for 13360 times since 2008 and has been extensively used amongst many experimental groups for battery life estimation that has resulted in 16 major publications.

Experiments upon the four battery sets were performed using ALCT under room temperature. The experiments were conducted until the batteries reached end-of-life (EOL) criteria. Failure is assumed when the battery reaches 70% of the rated capacity in the range of 2Ahr to 1.4Ahr. The battery dataset has been explored for estimating the state alongside the RUL prediction. Validation of current research results necessitates a substantial amount of experimental testing, which is both resource-intensive and time-consuming. Several battery research organizations have made their Li-ion datasets freely available for the larger community to analyze and compare. The developed data driven adaptive filtering prognostics framework has been once again applied over the capacity data obtained from the four Li-ion batteries (B0005, B0006, B0007, and B0018) for estimating the RUL. Keeping in mind about the majority of publication results, the double exponential fitting has been the preferred choice. The results of data fitting provide a broader range to the fitted coefficients. The domain has been reduced by generating space plots that helped in reducing the unnecessary computation. This is one of the major challenge in PF implementation and has been taken care of in the present work. The subsequent section elaborates the state prediction results along with the tabulated prognostics accuracy obtained by implementing the three PF variants upon the four batteries data.

6.3.1 Battery Data Set - B0005

The EOD as an estimated state along with the RUL for B0005 battery data has been evaluated. The training set amounts to 60% of the dataset, while1000particles have been used for predicting the state. The minimum value of the capacity is the failure threshold, which is represented by the horizontal line. RUL has been estimated within 95% confidence bounds.

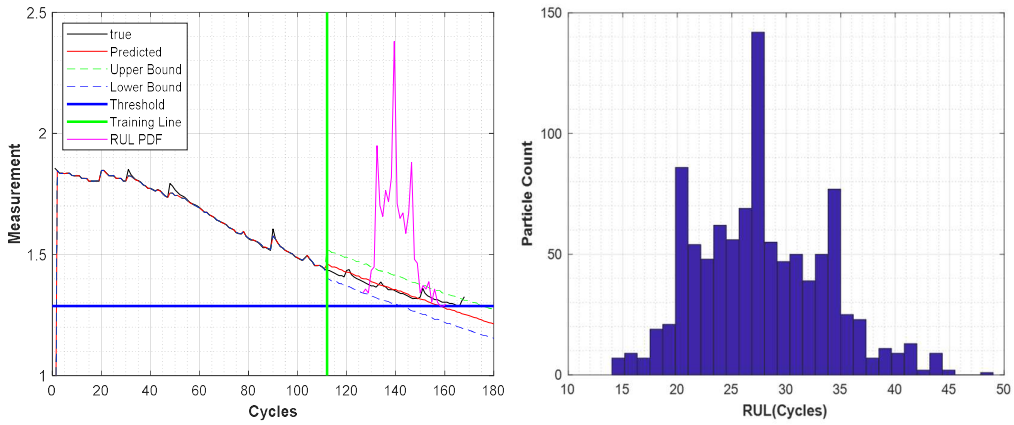

Figure 6.10 PF based (a) State prediction and (b) RUL estimation for B0005 battery

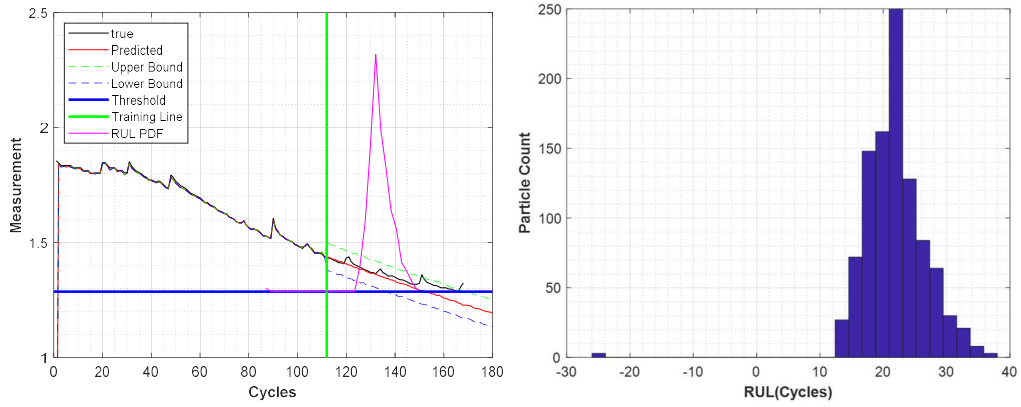

Figure 6.11 UPF based (a) State prediction and (b) RUL estimation for B0005 battery

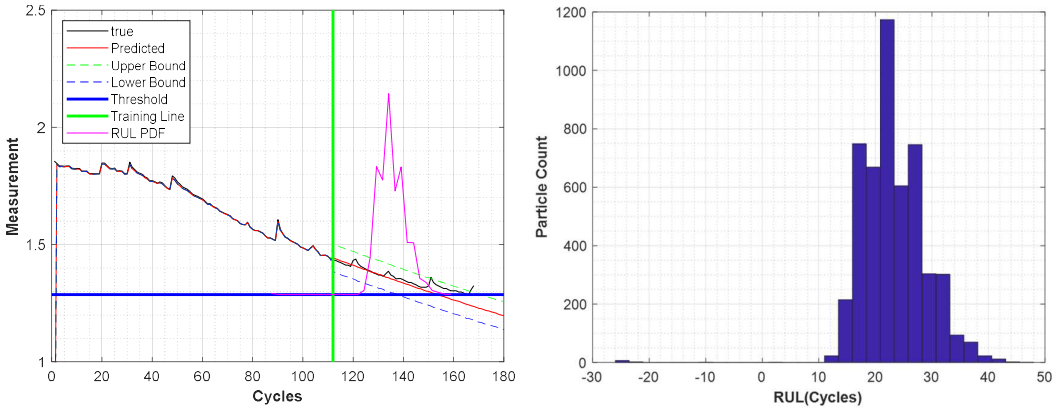

Figure 6.12 *i*-UPF based (a) State prediction and (b) RUL estimation for B0005 battery

Based on the above plots, accuracy results have been evaluated for 95% confidence bounds. The superiority of PF amongst all the three PF variants is seen.

Table 6.7 B0005-Prognostic Accuracy Results

B0005	*e*_PR	MSE	RMSE
PF	0.9998	8.6e-04	0.0013
UPF	0.9998	0.0016	0.0024
i-UPF	0.9999	0.0015	0.0023

6.3.2 Battery Data Set - B0006

The data from B0006 battery has been used for evaluating the EOD and the RUL. The RUL is evaluated when the state encounters 70% of the degradation in capacity. The algorithm uses 60% of the model coefficients for updating the estimated states beyond the vertical training line. Beyond the training line no model coefficients were updated.

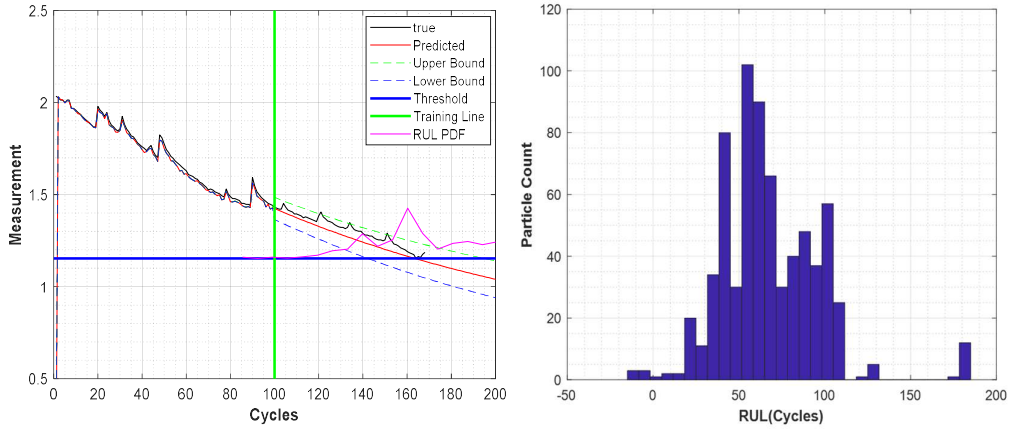

Figure 6.13 PF based (a) State prediction and (b) RUL estimation for B0006 battery

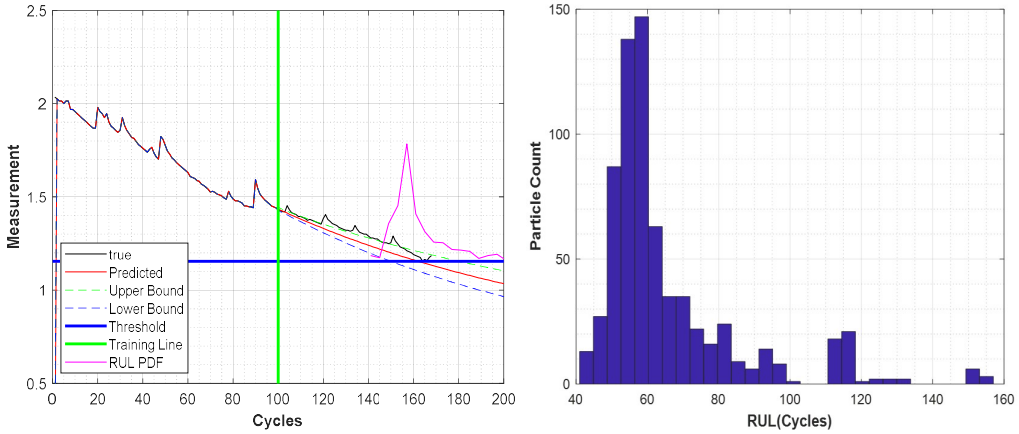

Figure 6.14 UPF based (a) State prediction and (b) RUL estimation for B0006 battery

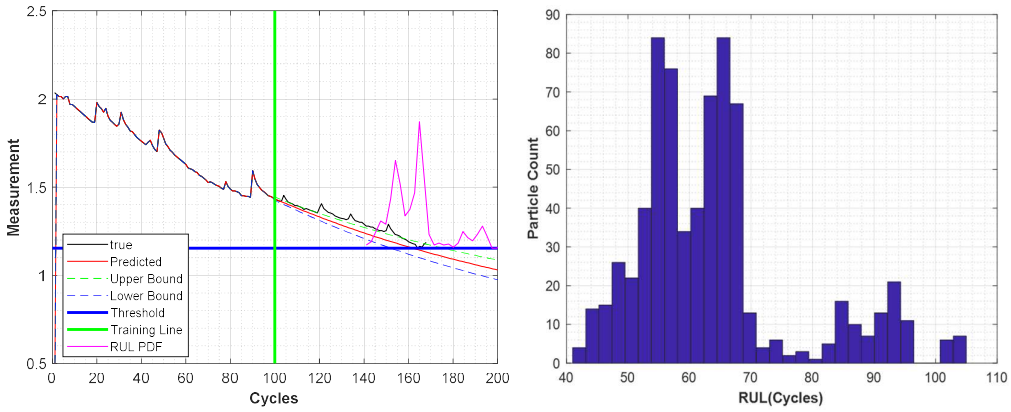

Figure 6.15 *i*-UPF based (a) State prediction and (b) RUL estimation for B0006 battery

The prognostics accuracy results illustrates that the *i*-UPF better predicts the RUL and the state for the present dataset.

Table 6.8 B0006-Prognostic Accuracy Results

B0006	*e*_PR	MSE	RMSE
PF	0.9993	0.0074	0.0125
UPF	0.9999	2.7e-04	4.4e-04
i-UPF	0.9999	2.5e-04	4.1e-04

6.3.3 Battery Data Set - B0007

The same conditions for RUL and state prediction is followed for B0007 battery dataset. However, the computational accuracy was found to increase with the use of 500 particles.

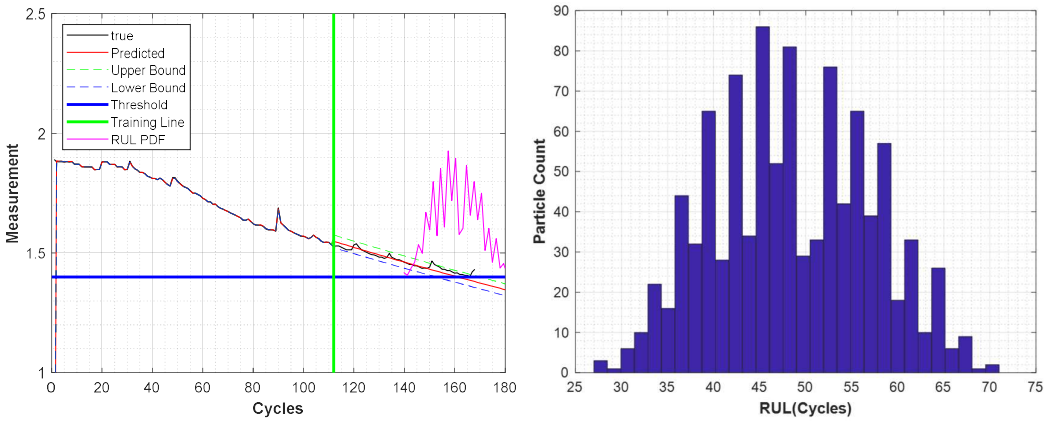

Figure 6.16 PF based (a) State prediction and (b) RUL estimation for B0007 battery

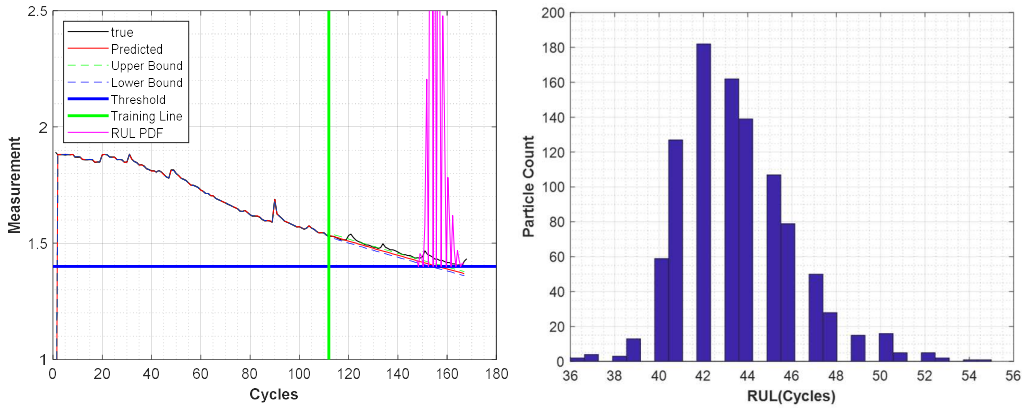

Figure 6.17 UPF based (a) State prediction and (b) RUL estimation for B0007 battery

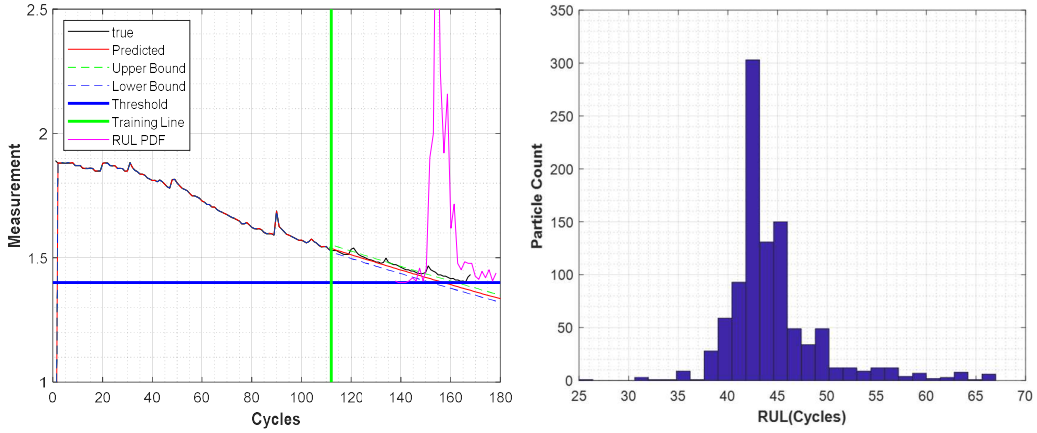

Figure 6.18 *i*-UPF based (a) State prediction and (b) RUL estimation for B0007 battery

Keeping all other parameters the same as in the above two cases, the *i*-UPF has been found to be accurate in the RUL prediction.

Table 6.9 B0007-Prognostic Accuracy Results

B0007	*e*_PR	MSE	RMSE
PF	0.9988	2.2e-04	3.4e-04
UPF	0.9980	1.1e-04	1.7e-04
i-UPF	0.9999	2.1e-04	3.2e-04

6.3.4 Battery Data Set - B0018

The B0018 dataset has been one of the challenging datasets with very high peaks. The presently developed strategy of *i*-UPF has been able to counter all the challenges and yield highly superior results.

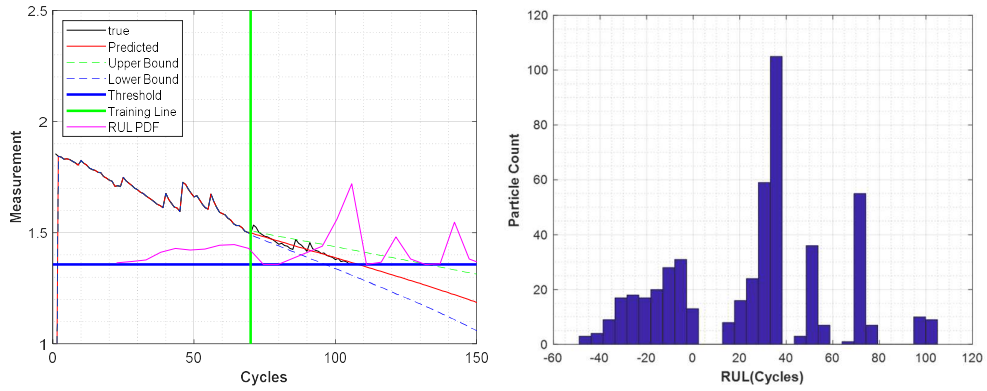

Figure 6.19 PF based (a) State prediction and (b) RUL estimation for B0018 battery

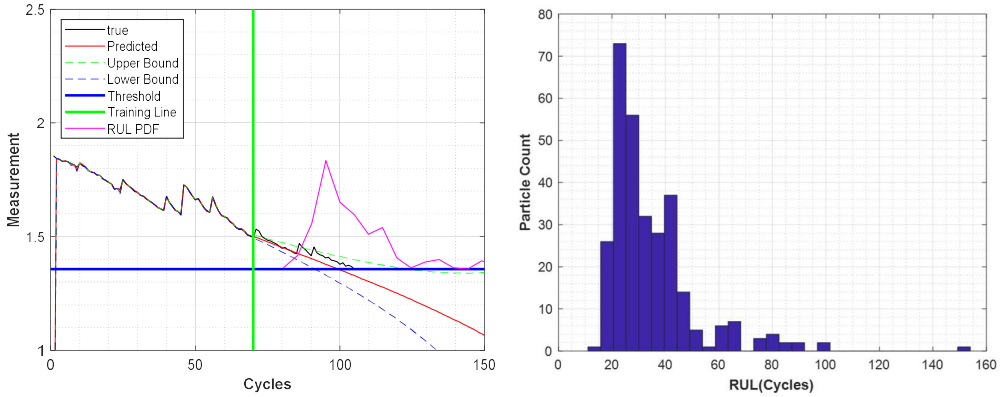

Figure 6.20 UPF based (a) State prediction and (b) RUL estimation for B0018 battery

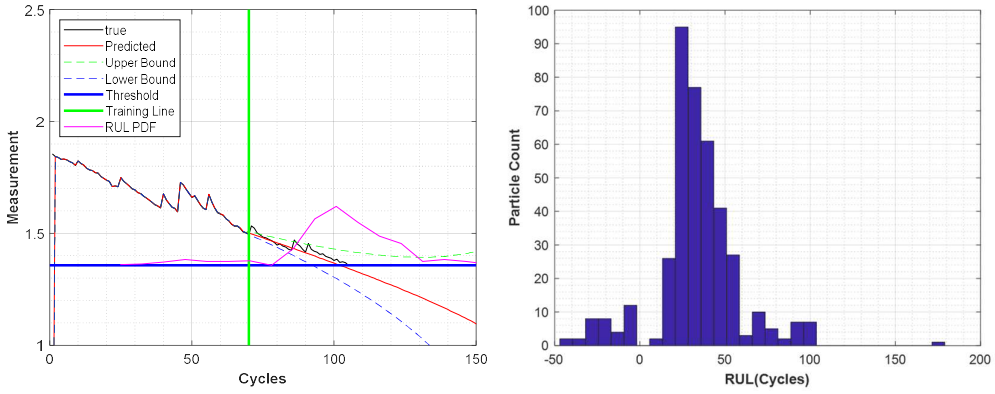

Figure 6.21 *i*-UPF based (a) State prediction and (b) RUL estimation for B0018 battery

The choice of parameter values once again explains the efficacy of our proposed algorithm. The dominance of *i*-UPF has been clearly demonstrated in the promising accuracy metrics which once again justifies our choice of implementing the proposed approach to the present problem.

Table 6.10 B0018-Prognostic Accuracy Results

B0018	*e*_PR	MSE	RMSE
PF	0.9999	1.4e-05	2.1e-05
UPF	0.9997	4.8e-04	7.3e-04
i-UPF	0.9999	5.8e-04	8.8e-04

6.4 Summary

The in-vitro clutch actuator data under three different working conditions has been made use of while predicting the RUL. The process of adaptive filtering makes use of the three PF variants, namely the PF, UPF and *i*-UPF for accurately and efficiently predicting the motor RUL. The PF is a state space approach that uses probabilistic samples for generating the approximated posterior density. Efficiency has been achieved through four resampling methods which is a correct approach to attain a valid sampling based representation of the probabilistic density. The comparative results of resampling were quantified for the three different experimental datasets by means of obtaining a higher estimate of ESS and a lower RUL_error value. The multinomial resampling had been the preferred choice while implementing UPF and *i*-UPF in all the three operations. The proposed *i*-UPF scheme makes use of *c*-value that helps in finalizing the two-step framework in selecting the number of particles that will be used for obtaining a posterior density. Hence, the resampling was followed by an appropriate choice of the *c*-value. Moreover, the error of RUL for *i*-UPF had been found to be much less in comparison to PF and UPF, with the ability to compute under lesser time. It was also evident from the mean value of RUL, that an appropriate choice of the *c*-value helped achieving a highly accurate estimate besides being computationally efficient.

In addition to the obtained results using the proposed approach, the present work also made use of the benchmark Li-ion battery data from the repository of the NASA Ames PCoE. The developed data driven adaptive filtering prognostics framework has been applied over the capacity data for estimating the RUL.